A genetically encoded fluorescent sensor of ERK activity

Christopher D. Harvey[a,b], Anka G. Ehrhardt[c], Cristina Cellurale[c], Haining Zhong[a], Ryohei Yasuda[d], Roger J. Davis[c], and Karel Svoboda[a,b,1]

[a]Janelia Farm Research Campus, Howard Hughes Medical Institute, Ashburn, VA 20147; [b]Watson School of Biological Sciences, Cold Spring Harbor Laboratory, Cold Spring Harbor, NY 11724; [c]Howard Hughes Medical Institute and Program in Molecular Medicine, University of Massachusetts Medical School, Worcester, MA 01605; and [d]Neurobiology Department, Duke University, Durham, NC 27710

Edited by Solomon H. Snyder, Johns Hopkins University School of Medicine, Baltimore, MD, and approved October 16, 2008 (received for review May 13, 2008)

The activity of the ERK has complex spatial and temporal dynamics that are important for the specificity of downstream effects. However, current biochemical techniques do not allow for the measurement of ERK signaling with fine spatiotemporal resolution. We developed a genetically encoded, FRET-based sensor of ERK activity (the extracellular signal-regulated kinase activity reporter, EKAR), optimized for signal-to-noise ratio and fluorescence lifetime imaging. EKAR selectively and reversibly reported ERK activation in HEK293 cells after epidermal growth factor stimulation. EKAR signals were correlated with ERK phosphorylation, required ERK activity, and did not report the activities of JNK or p38. EKAR reported ERK activation in the dendrites and nucleus of hippocampal pyramidal neurons in brain slices after theta-burst stimuli or trains of back-propagating action potentials. EKAR therefore permits the measurement of spatiotemporal ERK signaling dynamics in living cells, including in neuronal compartments in intact tissues.

fluorescence lifetime imaging microscopy | FRET | MAPK

The MAPK family is a class of serine/threonine kinases that includes the ERK, p38, and JNK subfamilies. Members of the ERK subfamily are essential for numerous, diverse physiological functions, including cellular differentiation, proliferation and neuronal plasticity, and their activities are up-regulated in many cancers (1). ERK signaling spans multiple subcellular compartments (1, 2). For example, in neurons ERK is activated at synapses and regulates gene transcription in the nucleus, hundreds of micrometers away (1). The spatial and temporal dynamics of ERK activity are likely critical in establishing the specificity of downstream signals. In PC12 cells, for example, epidermal growth factor (EGF) induces transient ERK activity only in the cytoplasm, leading to cellular proliferation; whereas, neural growth factor (NGF) triggers long-lasting ERK activity in both the cytoplasm and nucleus, resulting in cellular differentiation (2).

Traditional methods to measure ERK signaling, by Western blotting or immunostaining for phosphorylated, active ERK, have provided valuable insight into ERK function. However, these methods present a static snapshot of cellular events; they do not allow for the dynamic examination of ERK activity with fine spatial resolution. Recently developed imaging approaches that use fluorescent sensors of signaling activities can overcome these shortcomings (3). FRET-based reporters have been used in living cells to monitor the spatiotemporal patterns of Ca^{2+} signaling and enzymatic activities (4). We therefore created a genetically encoded FRET-based sensor of ERK activity that selectively reports ERK signaling in living cells.

Results

Design and Function of EKAR. To create a genetically encoded fluorescent sensor of ERK activity, we customized a generic design for FRET-based kinase activity reporters (5–8). Our ERK activity sensor, named EKAR (extracellular signal-regulated kinase activity reporter), includes a fluorescent protein FRET pair well suited for 2-photon fluorescence lifetime imaging (2pFLIM; EGFP and mRFP1) (9, 10), a substrate phosphorylation peptide from Cdc25C containing the consensus MAPK target sequence (PRTP) (11), and the proline-directed WW phospho-binding domain (12) (Fig. 1). ERK activation leads to phosphorylation of the substrate sequence and subsequent binding by the phospho-binding domain. The resulting conformational rearrangement triggers a change in FRET between the donor (EGFP) and acceptor (mRFP1) fluorophores. Because specificity in MAPK signaling depends on docking domains (13), we added an ERK-specific, 4-aa (FQFP) docking site adjacent to the phosphorylation sequence (14). Finally, we included a central linker consisting of 72 glycine residues (15). EKAR expression was restricted to the nucleus likely because of the nuclear localization of the WW domain (16). Addition of a C-terminal nuclear export sequence resulted in cytoplasmic expression, providing a cytoplasmic form of the sensor ($EKAR_{cyto}$).

To test the sensor's function in living cells, HEK293 cells expressing EKAR were stimulated with EGF (100 ng/ml) to strongly activate ERK signaling. FRET was quantified and imaged by using 2pFLIM (9, 10, 17, 18). The fluorescence lifetime of the donor fluorophore (EGFP), defined as the average time between fluorophore excitation and photon emission, is related to FRET efficiency and the fraction of donors interacting with acceptors (binding fraction) (3). A shorter lifetime implies higher FRET. The fluorescence lifetime of $EKAR_{cyto}$ decreased rapidly following stimulation with EGF (ΔLifetime $= -2.92 \pm 0.07\%$, $P < 0.001$; Fig. 2 *A*, *B*, and *F*). In cells coexpressing $EKAR_{cyto}$ and $EKAR_{nuclear}$, the time courses and magnitudes of EGF-induced responses in the nucleus and cytoplasm were similar (Fig. 2*B*). We also measured the responses of a CFP-YFP version of $EKAR_{cyto}$, containing Cerulean (19) and Venus (20), by using intensity-based ratiometric methods. EGF stimulation triggered an increase in the ratio (R) of acceptor to donor fluorescence in HEK293 cells expressing this version of $EKAR_{cyto}$ ($\Delta R/R_{YFP/CFP} = 20.9 \pm 1.0\%$, $P < 0.001$; Fig. 2*C*). $EKAR_{cyto}$ therefore undergoes a stimulus-dependent FRET change.

The ERK-specific docking site (FQFP) was necessary for this FRET change. The inclusion of docking sites with lower affinities for ERK (14) greatly reduced the signal of $EKAR_{cyto}$ (Fig.

Author contributions: C.D.H., A.G.E., C.C., R.J.D., and K.S. designed research; C.D.H., A.G.E., and C.C. performed research; C.D.H., H.Z., R.Y., R.J.D., and K.S. contributed new reagents/analytic tools; C.D.H., A.G.E., and C.C. analyzed data; and C.D.H. and K.S. wrote the paper.

The authors declare no conflict of interest.

This article is a PNAS Direct Submission.

[1]To whom correspondence should be addressed. E-mail: svobodak@janelia.hhmi.org.

This article contains supporting information online at www.pnas.org/cgi/content/full/0804598105/DCSupplemental.

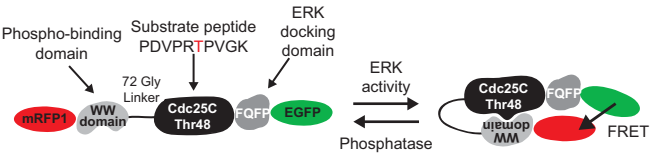

Fig. 1. Schematic of EKAR. ERK phosphorylation of EKAR triggers a conformational change and an increase in FRET between EGFP and mRFP1.

2*D*). Also, $EKAR_{cyto}$ with the 72-glycine-residue central linker had a larger signal than a version with a shorter Gly-rich linker (7) used in other sensors of this type ($\Delta Lifetime_{72\text{-}Gly} = -2.92 \pm 0.07\%$, $\Delta Lifetime_{short\ linker} = -1.72 \pm 0.18\%$, $P < 0.01$; Fig. 2*E*). Consistently, the 72-glycine linker also improved the signal of an EGFP-mRFP1 version of AKAR2 (21), a FRET-based sensor of PKA activity, in response to adenylate cyclase activation and phosphodiesterase inhibition in HEK293 cells ($\Delta Lifetime_{72\text{-}Gly} = -2.41 \pm 0.18\%$, $\Delta Lifetime_{short\ linker} = -1.45 \pm 0.29\%$, $P < 0.02$; Fig. 2*E*). Other components of EKAR, including the fluorescent proteins, phospho-binding domain and substrate peptide, were also optimized [see supporting information (SI) Table S1].

Relationship Between EKAR Signals and ERK Activity. To examine the relationship between ERK activation and the $EKAR_{cyto}$ signal, we mutated the MAPK phosphorylation site in the Cdc25C peptide (Thr-to-Ala substitution). The mutant sensor was insensitive to stimulation with EGF ($\Delta Lifetime = -0.08 \pm 0.11\%$, $P > 0.6$; Fig. 2*F*), indicating that the phosphorylation of the MAPK substrate peptide is necessary for the FRET change. In addition, preincubation with the ERK pathway inhibitor U0126 (10 μM) eliminated the EGF-induced decrease in fluorescence lifetime ($\Delta Lifetime = -0.05 \pm 0.09\%$, $P > 0.8$). Furthermore, application of U0126 following EGF-induced ERK activation caused a rapid (≈5 min) increase of the fluorescence lifetime to slightly above baseline levels (Fig. 2*F*). These results suggest that $EKAR_{cyto}$ reversibly reports ERK activity with rapid kinetics.

To examine further the relationship between $EKAR_{cyto}$ signals and ERK activity, we simultaneously measured ERK phosphorylation and $EKAR_{cyto}$ phosphorylation at the Cdc25C peptide by using a biochemical approach. Both ERK and $EKAR_{cyto}$ had low levels of baseline phosphorylation in COS7 cells (Fig. 3). Expression of a constitutively active form of MEK1 (ΔMEK1), to activate the ERK subfamily of MAPKs (22), caused a robust phosphorylation of both ERK and $EKAR_{cyto}$ (Fig. 3*A*). Overexpression of a MAPK phosphatase (MKP1), to inhibit ERK activation (23), eliminated phosphorylation of both $EKAR_{cyto}$ and ERK (Fig. 3*A*). Consistently, in the presence of ΔMEK1 or MKP1 $EKAR_{cyto}$-expressing cells had, on average, lower or higher fluorescence lifetimes, respectively, in comparison to control cells. Furthermore, stimulation of COS7 cells with phorbol myristate acetate (PMA, 1 μM) triggered strong phosphorylation of ERK and $EKAR_{cyto}$ that was prevented by the addition of the ERK pathway blocker U0126 (10 μM; Fig. 3*B*). The addition of PMA also triggered an ERK-dependent decrease in fluorescence lifetime (Fig. 3*B*). Therefore, $EKAR_{cyto}$ phosphorylation and $EKAR_{cyto}$ signals correlate with the activation of endogenous ERK.

Because the MAPK family members have similar target phosphorylation sequences, EKAR may also be sensitive to p38 and JNK activities, despite the inclusion of the ERK-specific docking domain. To address this possibility, we irradiated COS7 cells with UV light, which strongly induces p38 and JNK activity, while only modestly elevating ERK activity (Fig. S1) (24). UV irradiation triggered $EKAR_{cyto}$ phosphorylation that was eliminated in the presence of the ERK pathway blocker U0126 (10 μM) but was insensitive to p38 (10 μM PD169316) and JNK (10 μM SP600126) inhibitors (Fig. 3*C*). Consistently, UV irradiation decreased the fluorescence lifetime, on average, in $EKAR_{cyto}$-expressing cells in an ERK-dependent manner (Fig. 3*C*). $EKAR_{cyto}$ therefore selectively reports the activity of ERK and does not report the activities of closely related members of the MAPK family.

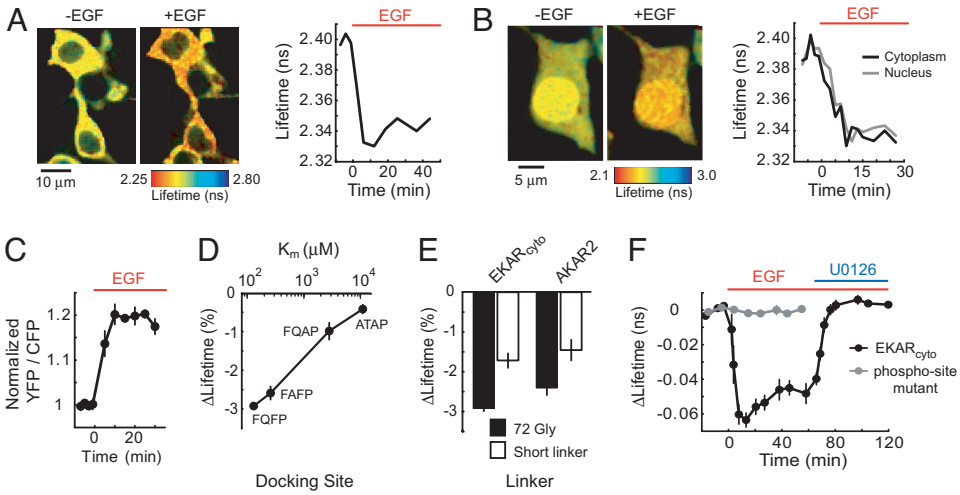

Fig. 2. Function of EKAR. (*A*) (*Left*) Fluorescence lifetime images of HEK293 cells transfected with $EKAR_{cyto}$ before (−5 min) and after (12 min) addition of EGF (100 ng/ml). (*Right*) Time course of the EGF-induced ERK activation. (*B*) (*Left*) Fluorescence lifetime images of HEK293 cells transfected with $EKAR_{cyto}$ and $EKAR_{nuclear}$ before (−4 min) and after (15 min) addition of EGF. EKAR concentration was higher in the nucleus. (*Right*) Time course of ERK activation in the nucleus and cytoplasm. (*C*) EGF-induced ERK activation, measured as the ratio of acceptor-to-donor fluorescence, in HEK293 cells expressing a CFP-YFP version of $EKAR_{cyto}$. Each region-of-interest (ROI) contained 2–6 cells. Data are mean ± SEM for 5 ROIs from 5 dishes. (*D*) EGF-induced lifetime changes in HEK293 cells expressing $EKAR_{cyto}$ variants containing docking sites with different affinities for ERK. K_m values are from ref. 14. Data for each docking site are mean ± SEM for ≥5 ROIs from 2 dishes. (*E*) Lifetime changes in HEK293 cells expressing central linker variants of $EKAR_{cyto}$ and an EGFP-mRFP1 version of AKAR2 after EGF stimuli or application of the adenylate cyclase activator forskolin (25 μM) and the phosphodiesterase inhibitor IBMX (100 μM), respectively. The sequence of the short glycine-rich linker is GNNGGNGGS (7) for EKAR and SAGKPGSGEGSTKG for AKAR2 (21). Data are mean ± SEM for ≥7 ROIs from ≥2 dishes for each condition. (*F*) EGF-induced lifetime changes for $EKAR_{cyto}$ and $EKAR_{cyto}$ mutated (Thr-to-Ala) at the phosphorylation site in the substrate peptide. For the wild type sensor, 10 μM U0126 was added 65 min after EGF application. Data are mean ± SEM for ≥9 ROIs from ≥2 dishes for each condition.

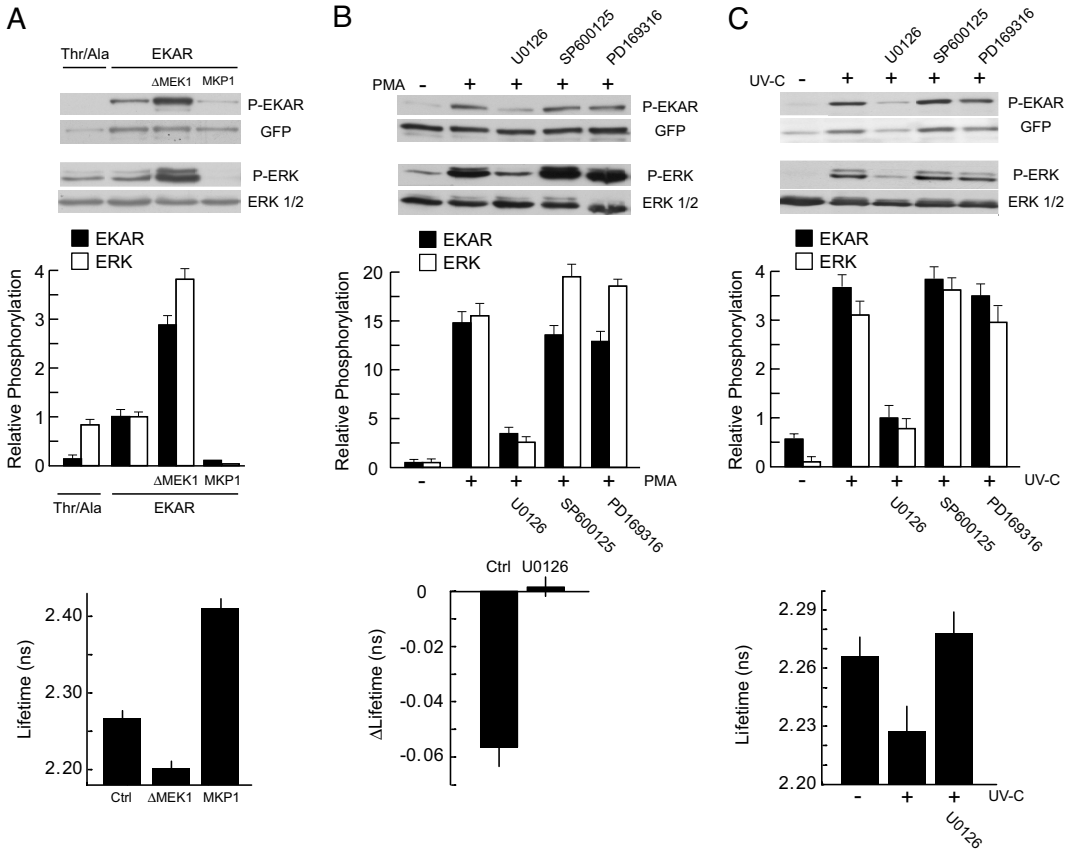

Fig. 3. Analysis of the relationship between ERK phosphorylation, EKAR phosphorylation, and EKAR signals. (*A*) Correlation between ERK phosphorylation, EKAR phosphorylation, and EKAR signals in COS7 cells. (*Top* and *Middle*) Cells were transfected with $EKAR_{cyto}$ or $EKAR_{cyto}$ (Thr-to-Ala). ERK activity was modulated by cotransfection with a constitutively active MEK (ΔMEK1) or a MAPK phosphatase (MKP1). An example Western blot is shown. Relative phosphorylation is the ratio of phosphorylated protein to total protein. Data are mean ± SEM from 3 experiments. (*Bottom*) Fluorescence lifetimes in cells expressing $EKAR_{cyto}$ in control, ΔMEK1, and MKP1 conditions. Data for each condition are mean ± SEM for >20 cells from 2 dishes. (*B*) PMA-induced ERK phosphorylation, EKAR phosphorylation, and EKAR signals in COS7 cells transfected with $EKAR_{cyto}$. Cells were stimulated with PMA (1 μM; 10 min). MAPK pathways were blocked by preincubation (30 min) with ERK (10 μM U0126), JNK (10 μM SP600125), and p38 (10 μM PD169316) pathway inhibitors. (*Top* and *Middle*) An example Western blot is shown. Data are mean ± SEM from 3 experiments. (*Bottom*) Changes in lifetime after PMA application with and without U0126 (10 μM). Data for each condition are mean ± SEM for 10 cells from 2 dishes. (*C*) UV irradiation-induced ERK phosphorylation, EKAR phosphorylation, and EKAR signals in COS7 cells transfected with $EKAR_{cyto}$. Cells were irradiated with 60 J/m^2 UV-C and then incubated for 1 h. Drugs are the same as in *B*. (*Top* and *Middle*) An example Western blot is shown. Data are mean ± SEM from 3 experiments. (*Bottom*) Fluorescence lifetimes in cells expressing $EKAR_{cyto}$ after UV-C treatment with and without U0126 (10 μM). Data for each condition are mean ± SEM for >20 cells from 2 dishes.

EKAR in Pyramidal Neurons. We also examined $EKAR_{cyto}$ function in pyramidal neurons in organotypic hippocampal brain slices. We monitored $EKAR_{cyto}$ signals in apical dendrites following high-frequency trains of back-propagating action potentials (40 action potentials at 83 Hz, repeated 8 times at 0.2 Hz), which cause relatively global Ca^{2+} influx through voltage-gated Ca^{2+} channels (VGCCs) to activate Ras (10, 25). VGCC-dependent Ca^{2+} influx triggered ERK activation in proximal dendrites, as reported by $EKAR_{cyto}$, that peaked within several minutes and decayed to baseline levels within 30 min ($\Delta Lifetime = -0.97 \pm 0.12\%$, $P < 0.01$; $t_{peak,\ ERK} = 5.5 \pm 0.7$ min; $\tau_{decay,\ ERK} = 10.7 \pm 1.1$ min, obtained by dividing the area by the peak amplitude of the transient; Fig. 4). The time course of ERK activation was longer than for Ras activation following the same stimulus ($t_{peak,\ Ras} < 2$ min; $\tau_{decay,\ Ras} = 4.7 \pm 0.6$ min) (10), which is consistent with ERK's role as a downstream effector of Ras. EKAR's sensitivity is therefore sufficient to study ERK signaling in neurons in intact tissue.

We used EKAR to study the dynamics of ERK signaling in the cytoplasm and nucleus of hippocampal pyramidal neurons in cultured brain slices. In neurons, ERK signals trigger downstream effects in both the cytoplasm and the nucleus (1). However, it is not known whether the dynamics and regulation of ERK activation are similar in these compartments. We therefore cotransfected pyramidal neurons with $EKAR_{cyto}$ and $EKAR_{nuclear}$ and used synaptic stimulation (5 stimuli at 100 Hz repeated 10 times at 5 Hz, all repeated 3 times at 0.1 Hz) to activate neurons in a theta-burst pattern (2–3 action potential bursts repeated at a theta frequency of 5 Hz), which mimics hippocampal firing patterns in awake animals and induces long-term potentiation (26). Theta-burst stimuli triggered robust ERK activation in the somatic cytoplasm and the nucleus ($\Delta Lifetime_{cytoplasm} = -0.88 \pm 0.04\%$, $\Delta Lifetime_{nucleus} = -0.83 \pm 0.05\%$; Fig. 5 *A–C*) with similar time courses; ERK activity peaked within 10 min ($t_{peak,\ cytoplasm} = 7.8 \pm 1.2$ min, $t_{peak,\ nuclear} = 8.4 \pm 1.0$ min, $P > 0.5$; Fig. 5 *B* and *C*) and decayed to baseline levels within 35 min ($\tau_{decay,\ cytoplasm} = 10.9 \pm 2.8$ min, $\tau_{decay,\ nuclear} = 14.7 \pm 2.1$ min, $P > 0.2$; Fig. 5 *A–C*). Previous studies suggest that ERK signaling may be preferentially activated by Ca^{2+} influx through L-type VGCCs (27–29). Application of the L-type VGCC blocker nimodipine (20 μM) reduced ERK activation to similar extents in the nucleus and cytoplasm ($\Delta Lifetime_{cytoplasm} = -0.54 \pm 0.08\%$, $\Delta Lifetime_{nucleus} = -0.63 \pm 0.08\%$, $P > 0.4$; Fig. 5*D*), indicating that Ca^{2+} influx

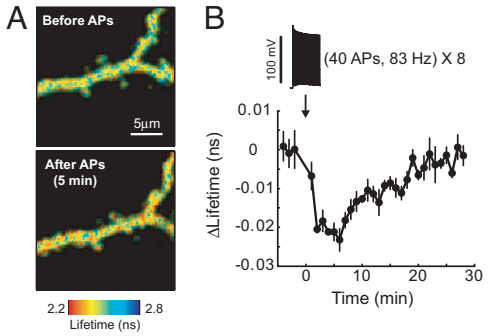

Fig. 4. EKAR function in hippocampal neurons. (*A*) Fluorescence lifetime images of dendrites from a pyramidal neuron in a cultured hippocampal brain slice before and after trains of back-propagating action potentials (40 APs at 83 Hz, repeated 8 times at 0.2 Hz). (*B*) Time course of ERK activity. Each ROI contained a ≈20-μm stretch of apical dendrite <70 μm from the soma. In the example image, the entire field of view was used as the ROI. Data are mean ± SEM for 7 cells.

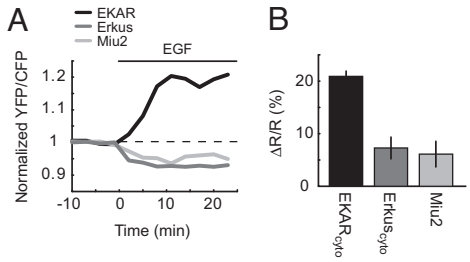

Fig. 6. Comparison of ERK activity reporters. (*A*) EGF-induced changes in the acceptor-to-donor fluorescence ratio in HEK293 cells expressing CFP-YFP versions of $EKAR_{cyto}$, $Erkus_{cyto}$, or Miu2. Example traces from individual experiments are shown. (*B*) Ratio changes for CFP-YFP versions of $EKAR_{cyto}$, $Erkus_{cyto}$, and Miu2 in HEK293 cells after EGF application. The ratio, *R*, was measured as the YFP/CFP ratio for $EKAR_{cyto}$ and the CFP/YFP ratio for $Erkus_{cyto}$ and Miu2. Data are mean ± SEM for ≥5 ROIs from 5 dishes.

through L-type VGCCs is an important trigger for ERK signaling. The dynamics and regulation of ERK activity following theta-burst stimuli are therefore similar in the somatic cytoplasm and nucleus, possibly because of action potential-evoked ERK activation by relatively global Ca^{2+} influx (30) and rapid diffusional exchange between the 2 compartments (31).

Comparison of ERK Activity Reporters. Several fluorescent indicators of ERK activity have been described previously (32–34). We compared the response of $EKAR_{cyto}$ with published reporters (Miu2 and Erkus) side-by-side in HEK293 cells stimulated with EGF. Miu2 consists of ERK tagged with CFP and YFP and undergoes a conformational change upon unbinding of MEK (33). Erkus is a sensor based on design principles similar to those used in EKAR, but with a different substrate peptide, phosphobinding domain, docking site, and linkers (34). EGF stimulation triggered small increases in the ratio of donor to acceptor fluorescence in cells expressing Miu2 or $Erkus_{cyto}$ ($\Delta R/R_{CFP/YFP,\ Miu2}$ = 6.1 ± 2.5%, $P < 0.05$; $\Delta R/R_{CFP/YFP,\ Erkus}$ = 7.3 ± 2.1%, $P < 0.01$; Fig. 6). The signal of $EKAR_{cyto}$ under the same conditions was approximately 3 times as large as those of Miu2 and $Erkus_{cyto}$ ($\Delta R/R_{YFP/CFP}$ = 20.9 ± 1.0%; versus Miu2: $P <$ 0.01; versus $Erkus_{cyto}$: $P < 0.01$; Fig. 6). Consistently, the fluorescence lifetime change for a mRFP1-EGFP version of Miu2 was smaller than that of $EKAR_{cyto}$ ($\Delta Lifetime_{Miu2}$ = +0.56 ± 0.16%, $\Delta Lifetime_{EKAR}$ = −2.92 ± 0.07%, $P < 0.01$; Table S1). EKAR is therefore likely preferable for monitoring ERK activity, especially in small compartments.

Signal-to-Noise Ratios of FLIM and Ratiometric FRET Measurements. We measured EKAR FRET signals by using both 2pFLIM (e.g., Fig. 2*A*) and intensity-based ratiometric measurements (Fig. 2*C*). Theory predicts that ratiometric methods may have a higher signal-to-noise ratio (SNR) than FLIM measurements (3, 35). We therefore used EKAR to compare the SNRs directly. We

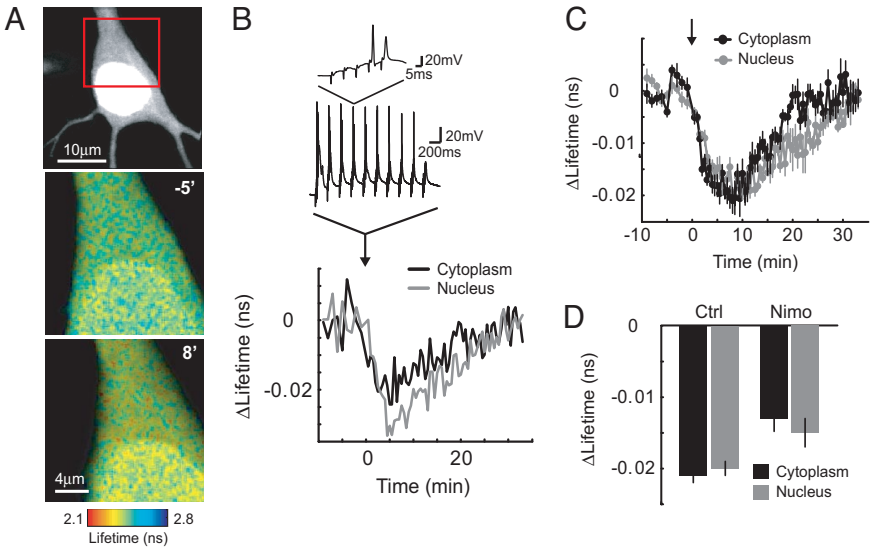

Fig. 5. ERK activation in the cytoplasm and nucleus after theta-burst stimuli. (*A*) (*Top*) GFP fluorescence image of a hippocampal pyramidal neuron expressing $EKAR_{cyto}$ and $EKAR_{nuclear}$ in a cultured brain slice. (*Middle* and *Bottom*) Fluorescence lifetime images of the same cell (boxed area). Images are from before (−5 min) and after (8 min) theta-burst stimuli. (*B*) Changes in lifetime in the cytoplasm and nucleus for the example shown in *A*. At time = 0, theta-burst stimuli (5 synaptic stimuli at 100 Hz, repeated 10 times at 5 Hz) were delivered 3 times with 10-second intervals. Example perforated patch recordings at the soma are shown. ROIs for the cytoplasm and nucleus were distinguished based on fluorescence intensity. (*C*) Time course of ERK activation in the nucleus and cytoplasm after theta-burst stimuli. Data are from 7 cells. (*D*) Lifetime changes following theta-burst stimuli in the nucleus and cytoplasm in the presence or absence of the L-type VGCC blocker nimodipine (20 μM). Lifetime changes were the average of 3 time points around the maximum change within 15 min of the stimulus. Data are from 7 and 6 cells for control and nimodipine conditions, respectively.

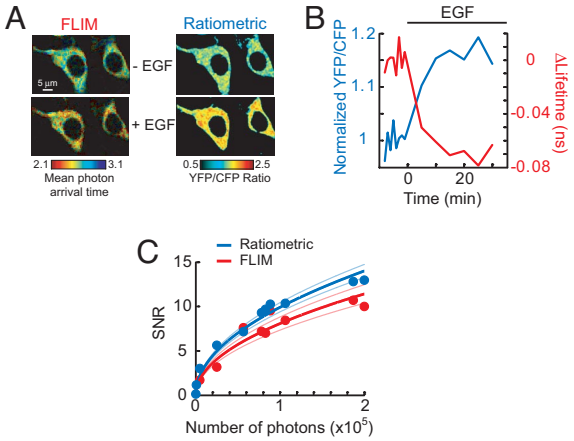

Fig. 7. Signal-to-noise ratios of FLIM and intensity-based FRET measurements. (*A*) FLIM and YFP/CFP ratio images of HEK293 cells transfected with a CFP-YFP version of $EKAR_{cyto}$ before and after EGF (100 ng/ml) application. The FLIM image is color-coded based on mean photon arrival times (see *SI Text*). (*B*) Lifetime (red) and ratio (blue) changes for the example shown in *A*. (*C*) SNRs of FLIM and ratiometric measurements at various numbers of donor photons (*N*). Each data point represents a single experiment; FLIM and intensity images were interleaved. The data were fitted by using the relationship $SNR \sim (N)^{1/2}$. Light blue and light red lines indicate the 95% confidence intervals.

acquired interleaved intensity and FLIM images of HEK293 cells expressing the CFP-YFP version of $EKAR_{cyto}$ before and after EGF stimulation (Fig. 7*A*). The excitation and fluorescence detection parameters were identical for both sets of images. No corrections were made for spectral bleed-through in the intensity images. The SNR was calculated as the EGF-induced change in YFP/CFP ratio ($\Delta R/R$) or fluorescence lifetime divided by the standard deviation of baseline fluctuations. Intensity-based measurements provided a slightly higher SNR than FLIM across a wide range of photon counts ($P < 0.05$; Fig. 7*C*), although the differences were surprisingly small ($< 20\%$). Therefore, intensity-based FRET measurements may be preferable to FLIM in certain experimental situations (see Discussion). We also attempted to compare SNRs using the EGFP-mRFP1 version of $EKAR_{cyto}$; however, the acceptor fluorescence of this sensor was too dim to provide a useable signal, likely because of the poor quantum yield of mRFP1 (36).

Discussion

We have designed and tested EKAR, a genetically encoded, FRET-based sensor of ERK activity. EKAR selectively and reversibly reported ERK activity after EGF stimulation in HEK293 cells and following back-propagating action potentials or theta-burst stimuli in hippocampal pyramidal neurons in brain slices. EKAR therefore allows for the analysis of ERK signaling in living cells.

Is EKAR's signal sufficient to address biological questions related to ERK signaling? We used EKAR to measure simultaneously the dynamics of ERK activity in the nucleus and cytoplasm of pyramidal neurons following physiological theta-burst stimuli (Fig. 5). Ca^{2+} influx through L-type VGCCs was an important trigger for ERK activity in both compartments (Fig. 5*D*). We also used EKAR in pyramidal neurons to monitor ERK activity in small dendrites following back-propagating action potentials (Fig. 4), and we measured EGF-induced ERK activation in 2 subcellular compartments simultaneously in HEK293 cells (Fig. 2*B*). EKAR responses in HEK293 cells following EGF stimulation had high SNRs even with modest numbers of photons (Fig. 7*C*), indicating that the SNR is sufficient to measure ERK activity following physiological stimuli and in small compartments with limited photon counts. Furthermore, the CFP-YFP version of $EKAR_{cyto}$ provided an acceptor-to-donor fluorescence ratio change of $\approx 20\%$ (Fig. 2*C*), which is comparable to those of other sensors, such as AKAR2 (21) and the CaMKII sensor Camuiα (37), that have been used to study the spatiotemporal dynamics of signaling events in living cells. We therefore conclude that EKAR's signal is sufficient to examine the spatial and temporal dynamics of ERK signaling under biologically relevant conditions in living cells. We note, however, that EKAR's signal is smaller than those of the best reporters, such as Ras sensors (10, 38) and AKAR3 (39). Also, as with all sensors, EKAR expression may perturb endogenous signaling, thus requiring experiments to measure sensor-dependent effects in each experimental preparation (4, 25, 40).

The design principles demonstrated here should be applicable to the design of similar kinase activity reporters. In particular, the addition of EKAR's central linker will likely improve the signals of other sensors of this type, including the PKC sensor CKAR (41), Src reporters (42), and reporters of receptor phosphorylation (6, 7), as we demonstrated for AKAR2 (Fig. 2*E*). Also, the inclusion of docking sites will aid the design of new, selective sensors for kinases with nonspecific substrate phosphorylation sequences, such as p38 and JNK (13).

We measured stimulus-induced EKAR FRET changes with both 2pFLIM and intensity-based ratiometric methods. Ratiometric FRET methods provided a slightly higher SNR than did FLIM measurements. It might therefore be advantageous to use ratiometric intensity methods in certain experimental situations, such as when using an intramolecular sensor to measure FRET signals before and after a stimulus in the same sample. However, under most experimental conditions, FLIM is likely preferable, especially for quantitative FRET measurements and comparisons of FRET across samples in light scattering tissue (3).

Materials and Methods

Sensor Construction. EKAR was assembled in the pCI vector (Promega) behind the CMV promoter. $EKAR_{nuclear}$ contains in the 5′ to 3′ direction: mRFP1 (36), the WW domain of Pin1 (amino acids 1–54 of human Pin1), a 72-glycine linker (3 24-Gly segments separated by Ala-Arg and Ala-Ser) (15), a Cdc25C peptide (PDVPRTPVGK, amino acids 43–52 of human Cdc25C) (43), the ERK docking site (FQFP) (14) and EGFP. The linkers adjacent to mRFP1 and EGFP are DLKL and RAREP, respectively. The nuclear export sequence of MEK (LQKKLEELELDE) (44) was included at the 3′ end of EGFP for $EKAR_{cyto}$. The CFP-YFP versions of $EKAR_{nuclear}$ and $EKAR_{cyto}$ were made by changing the fluorescent proteins to monomeric Cerulean (A206K mutation) (19) and monomeric Venus (A206K mutation) (20) at the N and C terminus, respectively. The linkers adjacent to Cerulean and Venus are RIH and PRAREI, respectively.

Preparations. HEK293 cells were cultured in DMEM with 10% FBS and were transfected with EKAR by using Lipofectamine 2000 (Invitrogen) or FuGENE (Roche). One-to-2 days after transfection, the cells were serum starved in 0.2% FBS overnight ($\approx$12 h). Imaging was carried out in a solution containing: 25 mM Hepes (pH 7.4), 114 mM NaCl, 2.2 mM KCl, 2 mM $CaCl_2$, 2 mM $MgCl_2$, 22 mM $NaHCO_3$, 1.1 mM NaH_2PO_4 and 2 mM glucose at room temperature. EGF (100 ng/ml final concentration, Calbiochem) was applied to cells plated in a 35-mm culture dish by using a pipette. Cells expressing AKAR2 were stimulated with an adenylate cyclase activator (25 μM forskolin) and a phosphodiesterase inhibitor (100 μM IBMX).

Hippocampal slice cultures were prepared from postnatal day 6–8 rats, as described (45), in accordance with the animal care and use guidelines of Cold Spring Harbor Laboratory and Janelia Farm Research Campus. After 5–8 days in culture, cells were transfected by ballistic gene transfer. Neurons were imaged 2 days after transfection in artificial cerebral spinal fluid (ACSF) containing: 127 mM NaCl, 2.5 mM KCl, 4 mM $CaCl_2$, 4 mM $MgCl_2$, 25 mM $NaHCO_3$, 1.25 mM NaH_2PO_4 and 25 mM glucose aerated with 95% O_2 and 5% CO_2 at room temperature.

Imaging and Electrophysiology. 2pFLIM was performed as described previously (10, 25). In brief, we used a custom-built 2-photon microscope with custom software integrated into ScanImage (46). A Ti:Sapphire laser tuned to 910 nm was used to excite EGFP for fluorescence lifetime measurements. Fluorescence

decay curves were measured by comparing the times of laser pulses (80 MHz) detected by a photodiode (FDS010; Thorlabs) and photon pulses from a fast PMT (H7422–40; Hamamatsu) by using a time-correlated single-photon counting board (SPC-730; Becker–Hickl) (10, 47). Red fluorescence photons were acquired simultaneously by using a second PMT (R3896; Hamamatsu). Only epifluorescence photons were collected. ''Green'' and ''red'' fluorescence photons were separated with a dichroic mirror (565 nm) and barrier filters (510/70, 635/90; Chroma). A similar setup was used for CFP-YFP EKAR imaging, except with 800-nm excitation light and different detection optics (dichroic mirror: 505 nm; filters: 480/40, 535/50).

Perforated patch-clamp recordings (Figs. 4 and 5), back-propagating action potential stimuli (Fig. 4), and synaptic stimulation (Fig. 5) were performed as previously described (10, 25, 48). See *SI Text* for details.

Biochemistry. $EKAR_{cyto}$-expressing COS7 cells were cotransfected with constitutively active MEK or MKP1, stimulated with 60 J/m^2 UV-C, or activated with 1 μM PMA (10 min). Standard Western blot analysis was performed. See *SI Text* for details.

Data Analysis. We used fluorescence lifetime measurements to quantify the FRET signals reported by EKAR. Fluorescence lifetimes were measured by using time-correlated single-photon counting following pulsed excitation, as described previously (10) (see *SI Text*).

Fluorescence lifetime changes were measured for the entire field-of-view, typically containing 2 or 3 HEK293 cells or a $\approx$20 μm stretch of pyramidal neuron dendrite. Because EGF was applied to HEK293 cells in a dish by using a pipette, the onset kinetics of the EKAR signal depended on both the diffusion of EGF to the cell of interest and the activation of ERK, resulting in large jitter of response onset times. We therefore calculated the lifetime change as the maximum lifetime change within 20 min after EGF application.

All *P* values are from 2-tailed *t* tests. The null hypothesis for all tests stated that the mean was equal to zero, except for the comparisons between linkers (Fig. 2*E*), sensors (Fig. 6*B*), and SNRs (Fig. 7*C*) for which the null hypothesis stated that the means were the same.

SNR Comparison of FLIM and Intensity-Based Measurements. Standard ratiometric and FLIM imaging methods were performed in HEK293 cells expressing the CFP-YFP version of $EKAR_{cyto}$. See *SI Text* and Fig. S2 for details.

ACKNOWLEDGMENTS. We thank B. Burbach, C. Zhang, H. White, B. Shields, S. Winfrey, and N. Ghitani for technical assistance; D. Yue (John Hopkins, Baltimore) for the glycine linker; D. Litchfield (University of Western Ontario, London, Ontario, Canada) for Pin1; D. Morrsion (National Cancer Institute, Rockville, MD) for Cdc25C; J. Blenis (Harvard Medical School, Boston) for murine RSK2; A. Miyawaki (RIKEN, Saitama, Japan) for the circularly permuted Venus variants; R. Tsien (University of California at San Diego, La Jolla, CA) for AKAR2; M. Matsuda (Osaka University, Osaka, Japan) for Miu2; and Y. Umezawa (University of Tokyo, Tokyo, Japan) for Erkus. This work was supported by the Howard Hughes Medical Institute, the National Institutes of Health, and a David and Fanny Luke Fellowship (to C.D.H.).

1. Thomas GM, Huganir RL (2004) MAPK cascade signalling and synaptic plasticity. *Nat Rev Neurosci* 5:173–183.
2. Marshall CJ (1995) Specificity of receptor tyrosine kinase signaling: transient versus sustained extracellular signal-regulated kinase activation. *Cell* 80:179–185.
3. Yasuda R (2006) Imaging spatiotemporal dynamics of neuronal signaling using fluorescence resonance energy transfer and fluorescence lifetime imaging microscopy. *Curr Opin Neurobiol* 16:551–561.
4. Miyawaki A (2003) Visualization of the spatial and temporal dynamics of intracellular signaling. *Dev Cell* 4:295–305.
5. Zhang J, Ma Y, Taylor SS, Tsien RY (2001) Genetically encoded reporters of protein kinase A activity reveal impact of substrate tethering. *Proc Natl Acad Sci USA* 98:14997–15002.
6. Ting AY, Kain KH, Klemke RL, Tsien RY (2001) Genetically encoded fluorescent reporters of protein tyrosine kinase activities in living cells. *Proc Natl Acad Sci USA* 98:15003–15008.
7. Sato M, *et al.* (2002) Fluorescent indicators for imaging protein phosphorylation in single living cells. *Nat Biotechnol* 20:287–294.
8. Ni Q, Titov DV, Zhang J (2006) Analyzing protein kinase dynamics in living cells with FRET reporters. *Methods* 40:279–286.
9. Peter M, *et al.* (2005) Multiphoton-FLIM quantification of the EGFP-mRFP1 FRET pair for localization of membrane receptor-kinase interactions. *Biophys J* 88:1224–1237.
10. Yasuda R, *et al.* (2006) Supersensitive Ras activation in dendrites and spines revealed by two-photon fluorescence lifetime imaging. *Nat Neurosci* 9:283–291.
11. Gonzalez FA, Raden DL, Davis RJ (1991) Identification of substrate recognition determinants for human ERK1 and ERK2 protein kinases. *J Biol Chem* 266:22159–22163.
12. Lu PJ, Zhou XZ, Shen M, Lu KP (1999) Function of WW domains as phosphoserine- or phosphothreonine-binding modules. *Science* 283:1325–1328.
13. Bardwell L (2006) Mechanisms of MAPK signalling specificity. *Biochem Soc Trans* 34:837–841.
14. Jacobs D, *et al.* (1999) Multiple docking sites on substrate proteins form a modular system that mediates recognition by ERK MAP kinase. *Genes Dev* 13:163–175.
15. Mori MX, Erickson MG, Yue DT (2004) Functional stoichiometry and local enrichment of calmodulin interacting with Ca2+ channels. *Science* 304:432–435.
16. Lu PJ, *et al.* (2002) Critical role of WW domain phosphorylation in regulating phosphoserine binding activity and Pin1 function. *J Biol Chem* 277:2381–2384.
17. Piston DW, Sandison DR, Webb WW (1992) in *Time-Resolved Laser Spectroscopy in Biochemistry III*, ed Lakowicz J R (SPIE, Bellingham, WA), pp 379–389.
18. Gratton E, *et al.* (2003) Fluorescence lifetime imaging for the two-photon microscope: Time-domain and frequency-domain methods. *J Biomed Opt* 8:381–390.
19. Rizzo MA, Springer GH, Granada B, Piston DW (2004) An improved cyan fluorescent protein variant useful for FRET. *Nat Biotechnol* 22:445–449.
20. Nagai T, *et al.* (2002) A variant of yellow fluorescent protein with fast and efficient maturation for cell-biological applications. *Nat Biotechnol* 20:87–90.
21. Zhang J, *et al.* (2005) Insulin disrupts beta-adrenergic signalling to protein kinase A in adipocytes. *Nature* 437:569–573.
22. Mansour SJ, *et al.* (1994) Transformation of mammalian cells by constitutively active MAP kinase kinase. *Science* 265:966–970.
23. Sun H, Charles CH, Lau LF, Tonks NK (1993) MKP-1 (3CH134), an immediate early gene product, is a dual specificity phosphatase that dephosphorylates MAP kinase in vivo. *Cell* 75:487–493.
24. Davis RJ (2000) Signal transduction by the JNK group of MAP kinases. *Cell* 103:239–252.
25. Harvey CD, Yasuda R, Zhong H, Svoboda K (2008) The spread of Ras activity triggered by activation of a single dendritic spine. *Science* 321:136–140.
26. Larson J, Wong D, Lynch G (1986) Patterned stimulation at the theta frequency is optimal for the induction of hippocampal long-term potentiation. *Brain Res* 368:347–350.
27. Wu GY, Deisseroth K, Tsien RW (2001) Spaced stimuli stabilize MAPK pathway activation and its effects on dendritic morphology. *Nat Neurosci* 4:151–158.
28. Dolmetsch RE, *et al.* (2001) Signaling to the nucleus by an L-type calcium channel-calmodulin complex through the MAP kinase pathway. *Science* 294:333–339.
29. Dudek SM, Fields RD (2002) Somatic action potentials are sufficient for late-phase LTP-related cell signaling. *Proc Natl Acad Sci USA* 99:3962–3967.
30. Adams JP, Dudek SM (2005) Late-phase long-term potentiation: getting to the nucleus. *Nat Rev Neurosci* 6:737–743.
31. Wiegert JS, Bengtson CP, Bading H (2007) Diffusion and not active transport underlies and limits ERK1/2 synapse-to-nucleus signaling in hippocampal neurons. *J Biol Chem* 282:29621–29633.
32. Green HM, Alberola-Ila J (2005) Development of ERK activity sensor, an in vitro, FRET-based sensor of extracellular regulated kinase activity. *BMC Chem Biol* 5:1.
33. Fujioka A, *et al.* (2006) Dynamics of the Ras/ERK MAPK cascade as monitored by fluorescent probes. *J Biol Chem* 281:8917–8926.
34. Sato M, Kawai Y, Umezawa Y (2007) Genetically encoded fluorescent indicators to visualize protein phosphorylation by extracellular signal-regulated kinase in single living cells. *Anal Chem* 79:2570–2575.
35. Neher RA, Neher E (2004) Applying spectral fingerprinting to the analysis of FRET images. *Microsc Res Tech* 64:185–195.
36. Campbell RE, *et al.* (2002) A monomeric red fluorescent protein. *Proc Natl Acad Sci USA* 99:7877–7882.
37. Takao K, *et al.* (2005) Visualization of synaptic Ca2+/calmodulin-dependent protein kinase II activity in living neurons. *J Neurosci* 25:3107–3112.
38. Mochizuki N, *et al.* (2001) Spatio-temporal images of growth-factor-induced activation of Ras and Rap1. *Nature* 411:1065–1068.
39. Allen MD, Zhang J (2006) Subcellular dynamics of protein kinase A activity visualized by FRET-based reporters. *Biochem Biophys Res Commun* 348:716–721.
40. Neher E, Augustine GJ (1992) Calcium gradients and buffers in bovine chromaffin cells. *J Physiol* 450:273–301.
41. Violin JD, Zhang J, Tsien RY, Newton AC (2003) A genetically encoded fluorescent reporter reveals oscillatory phosphorylation by protein kinase C. *J Cell Biol* 161:899–909.
42. Wang Y, *et al.* (2005) Visualizing the mechanical activation of Src. *Nature* 434:1040–1045.
43. Verdecia MA, *et al.* (2000) Structural basis for phosphoserine-proline recognition by group IV WW domains. *Nat Struct Biol* 7:639–643.
44. Fukuda M, Gotoh I, Gotoh Y, Nishida E (1996) Cytoplasmic localization of mitogen-activated protein kinase kinase directed by its NH2-terminal, leucine-rich short amino acid sequence, which acts as a nuclear export signal. *J Biol Chem* 271:20024–20028.
45. Stoppini L, Buchs PA, Muller DA (1991) A simple method for organotypic cultures of nervous tissue. *J Neurosci Methods* 37:173–182.
46. Pologruto TA, Sabatini BL, Svoboda K (2003) ScanImage: Flexible software for operating laser-scanning microscopes. *Biomed Eng Online* 2:13.
47. Lakowicz JR (1999) *Principles of Fluorescence Spectroscopy* (Plenum, New York).
48. Harvey CD, Svoboda K (2007) Locally dynamic synaptic learning rules in pyramidal neuron dendrites. *Nature* 450:1195–1200.

Supporting Information

Harvey *et al.* 10.1073/pnas.0804598105

SI Methods

Electrophysiology. Perforated patch-clamp recordings, which prevent the washout of signaling molecules, were performed with a pipette solution containing: 136.5 mM potassium gluconate, 17.5 mM KCl, 9 mM NaCl, 1 mM $MgCl_2$, 10 mM Hepes (pH 7.2), 0.2 mM EGTA and 0.5 mg mL^{-1} amphotericin B (1, 2). Pipettes were front-filled with a small volume of solution lacking amphotericin B. Experiments were performed when the access resistance dropped below 60 MΩ (≈30 min after seal formation). Back-propagating action potentials (Fig. 4) were triggered by current injections (2–4 nA, 2 ms) at the soma. Glutamate receptor blockers (10 μM NBQX and 5 μM CPP) were included in the bath during back-propagating action potential experiments. Synaptic stimulation (Fig. 5) was performed using short current pulses (0.1 ms) delivered with a glass pipette (≈2- to 3-μm tip diameter) filled with ACSF. The pipette was positioned in the apical dendrites ≈150 μm from the soma. The stimulus strength was set to produce an excitatory postsynaptic potential (EPSP) of ≈5–8 mV. The theta-burst protocol consisted of a burst of 5 synaptic stimuli at 100 Hz, repeated 10 times at 5 Hz. The set of 10 bursts was repeated 3 times at 10-second intervals. Picrotoxin (100 μm), to prevent inhibition, and 2-chloroadenosine (2 μm), to reduce recurrent activity, were included in the bath during synaptic stimulation.

Biochemistry. COS7 cells were cultured in DMEM with 10% FBS and were transfected with $EKAR_{cyto}$ using Lipofectamine. The expression vectors for constitutively active MEK (DN-MEK-EE) and MKP1 have been described previously (3, 4). For UV treatment (Fig. 3*C*), cells were irradiated with 60 J/m^2 UV-C and then incubated for 1 h before lysis. For PMA stimulation experiments (Fig. 3*B*), cells were serum-starved for 12 h starting at 36 h after transfection and were lysed following PMA application (1 μM, 10 min). The lysis buffer contained: 25 mM Hepes (pH 7.5), 134 mM NaCl, 10% glycerol, 1% Triton X-100, 25 mM β-glycerophosphate, 2 mM EDTA, 100 μM Na orthovanadate, 10 mM PMSF, 10 μg/ml leupeptin and 10 μM aprotinin. Western blots were analyzed using chemiluminescence detection and were quantified in ImageJ. $EKAR_{cyto}$ phosphorylation was measured at its Cdc25C substrate peptide. Phospho-Cdc25C signals from $EKAR_{cyto}$ and from endogenous Cdc25C were distinguished based on protein size. Relative phosphorylation was calculated as the ratio of phosphorylated protein to total protein from the same sample; each intensity measurement is therefore independent of sample-to-sample variations in protein levels. The antibodies used were: GFP (Roche), ERK1/2 (Santa Cruz Biotechnology), *p*-ERK1/2 (Cell Signaling Technology), *p*-JNK (Cell Signaling Technology), *p*-p38 (Cell Signaling Technology), and *p*-Thr-48-Cdc25C (Cell Signaling Technology). Phorbol myristate acetate (PMA) was purchased from Sigma. U0126, SP600125, and PD169316 were purchased from Calbiochem. U0126, SP600125, and PD169316 (a pyridinyl imidazole compound similar to SB203580) are selective antagonists of MKK1, JNK, and p38, respectively (5, 6).

FLIM Data Analysis. We used fluorescence lifetime measurements to quantify the FRET signals reported by EKAR. Following pulsed excitation with a mode-locked Ti:sapphire laser (80-MHz pulse frequency), a fluorescence decay curve, $F(t)$, was obtained from a histogram of photon arrival times, measured as the time between photon signals and laser pulses using time-correlated single photon counting (TCSPC) (1, 7, 8). The fluorescence lifetime can be obtained from the mean photon arrival time, where the mean photon arrival time, $\langle t \rangle$, is measured as (7):

$$\langle t \rangle = \frac{\int dt \cdot tF(t)}{\int dt \cdot F(t)} \quad [1]$$

The mean photon arrival time is related to the fluorescence lifetime, $\langle \tau \rangle$, by an offset arrival time, t_o, that depends on the position of the sample:

$$\langle \tau \rangle = \langle t \rangle - t_0 \quad [2]$$

First it is necessary to estimate the offset arrival time. We therefore calculated the fluorescence lifetime from a fit of the fluorescence decay curve. We assumed that the fluorescence decay curve, $F(t)$, was composed of 2 populations, free donors (P_D) and donors bound to acceptor (P_{AD}), with fluorescence lifetimes τ_D and τ_{AD}, respectively:

$$F(t) = F_o[P_D \exp(-t/\tau_D) + P_{AD} \exp(-t/\tau_{AD})] \quad [3]$$

However, in TCSPC measurements, the fluorescence decay curve is convolved with the pulse response function (PRF) of the microscope, which is the uncertainty in the arrival times of photons mostly due to the transit time spread of the PMT (assumed to be Gaussian with width τ_G) (1). The fluorescence decay curve therefore can be expressed as:

$$F(t,t_0, \tau_D, \tau_G, \tau_{AD}, P_D, P_{AD}) = F_0[P_D \cdot G(t, t_0, \tau_D, \tau_G) + P_{AD} \cdot G(t, t_0, \tau_{AD}, \tau_G)] \quad [4]$$

where G is the convolution of the Gaussian PRF and an exponential decay:

$$G(t, t_0, \tau_D, \tau_G) = \frac{1}{2} \exp\left(\frac{\tau_G^2}{2\tau_D} - \frac{t - t_0}{\tau_D}\right) \operatorname{erf}\left(\frac{\tau_G^2 - \tau_D(t - t_0)}{\sqrt{2}\tau_D \tau_G}\right) \quad [5]$$

We fit Eq. **4** with 2 exponentials with time constants τ_D and τ_{AD}. The fit was constrained by fixing τ_D and τ_G to values obtained under favorable conditions in HEK293 (τ_D = 2.53 ns for EGFP and 3.02 ns for Venus, and τ_G = 0.157 ns) (1). From the fit, we calculated the mean fluorescence lifetime, where the theoretical average for multiple populations (i.e., free donors and donors bound to acceptors) is given by:

$$\langle \tau \rangle \sim \frac{\int dt \cdot [P_D \cdot \exp(-t/\tau_D) + P_{AD} \cdot \exp(-t/\tau_{AD})]}{\int dt \cdot [P_D \cdot \exp(-t/\tau_D) + P_{AD} \cdot \exp(-t/\tau_{AD})]} \sim \frac{P_D \tau_D^2 + P_{AD} \tau_{AD}^2}{P_D \tau_D + P_{AD} \tau_{AD}} \quad [6]$$

For each experiment, we calculated the fluorescence lifetime for multiple images (range 3–4) by fitting in this manner and

compared these values with the mean photon arrival times to estimate the offset arrival time using Eq. **2**. The average offset arrival time was used for all images in an experiment. All fluorescence lifetime values were then obtained from the mean photon arrival time (Eq. **1**) using the calculated offset (Eq. **2**). This method was also used to estimate the fluorescence lifetime of the CFP-YFP version of EKAR (Table S1), even though Cerulean has a fluorescence decay curve with multiple time constants (1).

In certain experimental cases, determining the fluorescence lifetime and binding fraction (P_{AD}) from fitting is preferable to using the mean photon arrival time (1). With sensors like EKAR, however, 3 populations of donors with different lifetimes are present: donors not bound to acceptors, donors bound to acceptors, and donors in a molecule without a functional acceptor chromophore. The third population is likely a significant fraction of the sensor molecules because only ≈50% of mRFP1 molecules function as acceptors (1). Since fitting can be unstable with 3 populations, the mean photon arrival time method therefore is preferable here.

SNR Comparison of FLIM and Intensity-Based Measurements. HEK293 cells were transfected with the CFP-YFP version of $EKAR_{cyto}$ and stimulated with EGF, as described above. For each sample, FLIM images and intensity images were interleaved and acquired following 2-photon excitation with 800-nm light. The excitation and detection parameters were identical for both sets of images. For intensity-based measurements, the SNR was defined as the maximum YFP/CFP ratio change, normalized to the baseline ratio ($\Delta R/R$), divided by the standard deviation of $\Delta R/R$ for baseline images. No corrections were made for spectral bleed-through. For FLIM measurements, the SNR was defined as the maximum fluorescence lifetime change divided by the standard deviation of the baseline fluorescence lifetime changes. Eight baseline time points were acquired for each experiment. The maximum ratio and lifetime changes were obtained within 20 min after the addition of EGF.

Ratio images (Fig. 7*A*) were created by dividing the YFP signal by the CFP signal pixel-by-pixel following low-pass filtering of the YFP and CFP images. Only pixels with a value greater than the mean background signal plus 4 times the standard deviation of the background signal were included in the ratio images. CFP FLIM images were created using only the mean photon arrival time, without correction for the sample position using an offset arrival time, t_o. Because Cerulean has a fluorescence decay curve with multiple time constants even in the absence of acceptor (1), stable curve-fitting to estimate the fluorescence lifetime and the offset arrival time were not possible. Since the offset arrival time is constant for a given sample, the absolute changes in the mean photon arrival time are the same as the absolute changes in fluorescence lifetime (see Eq. **2**). Therefore, CFP FLIM images (Fig. 7*A*) illustrate the fluorescence lifetime changes, but the values provided (in nanoseconds) are mean photon arrival times and do not accurately reflect fluorescence lifetime values.

SI Discussion

Optimization of EKAR's Signal. The mature form of EKAR resulted from a screen of numerous sensors, using the EGF stimulation of HEK293 cells as a fast and robust assay to optimize the components of EKAR (i.e., FRET pairs, phospho-binding domains, substrate peptides, and linkers). See Table S1 for a summary of the sensors tested.

The EGFP-mRFP1 FRET pair was selected because it is a combination well-suited for 2pFLIM (9) that provided a large fluorescence lifetime change. Other fluorescent protein combinations, such as circularly permuted forms of Venus (10–12) paired with mRFP1, provided minor improvements in the signal (Table S1). However, because EGFP was brighter than Venus under 2-photon excitation in our setup (1), we chose the EGFP-mRFP1 pair. Other FRET pairs, such as Venus-mRFP1, Venus-hcRed, and EGFP-mCherry, did not provide larger signals. For ratiometric FRET measurements, other FRET pairs, such as CFP-YFP combinations, may be preferable (Fig. 2*C*). Also, the incorporation of new FRET pairs (13, 14) may improve EKAR's signal.

Several phospho-binding domains and substrate peptides were tested. The WW domain-Cdc25C peptide combination provided the largest signal while maintaining rapid reversibility. The binding affinity between these 2 domains ($K_D \approx 8\ \mu M$) (15) is a major determinant of reversibility, such that low affinities allow phosphatases to act on the sensor (16). Low affinities therefore produce sensors with kinetics that resemble the activity patterns of the endogenous kinase. High affinities can also be useful to produce irreversible sensors with larger signals for cases in which the activity kinetics are not important. This situation is similar to the use of indicators with differing affinities in $[Ca^{2+}]$ imaging (17). Because the crystal structure of the WW-phosphopeptide interface has been solved (15), the design of EKAR variants with a broad range of affinities should be possible. Other less successful combinations were also tested: the Cdc25C peptide paired with the FHA phospho-binding domain and the ERK substrate RSK2 (amino acids 560–740) combined with the WW domain.

Optimization of the linker regions greatly enhanced the sensor's signal. In addition to optimizing the central linker (Fig. 2*E*), we also varied the length of the linkers adjacent to the fluorescent proteins. We found that shorter linkers, consisting of only several amino acids, provided the largest signals. Finally, we attempted to decrease the baseline FRET by modifying the central linker to increase the distance between the fluorescent proteins (18). However, the placement of rigid α-helices or α-helices in combination with flexible linkers was unsuccessful in this aim.

Different sensor designs were also tested. First, ERK undergoes a conformational change upon activation due to the unbinding of MEK (19). Such a conformational change may alter FRET. However, placement of mRFP1 and EGFP at the N and C terminus of ERK, respectively, resulted in only a small FRET change upon EGF stimulation. Second, ERK may dimerize upon activation (20). We made an intramolecular sensor containing mRFP1-ERK and EGFP-ERK joined by a flexible linker; however, this sensor showed no stimulus-dependent FRET change.

Comparison of Ratio and Lifetime Changes with FRET. EKAR undergoes a ≈2–3% decrease in fluorescence lifetime and a ≈20% increase in acceptor-to-donor fluorescence ratio following various stimuli (e.g., Fig. 2). Is this relationship between lifetime and ratio changes expected for a FRET change? We estimated the relationship between percent ratio and lifetime changes following increases in binding fraction (P_{AD}). In ratiometric measurements, the fluorescence in the donor (F_D) and acceptor (F_{AD}) channels can be calculated as (21):

$$F_D = F_D^{\text{no FRET}}(1 - Y_{\text{FRET}} \cdot P_{AD}) \quad [7]$$

$$F_A = F_D^{\text{no FRET}} \cdot \alpha \cdot Y_{\text{FRET}} \cdot P_{AD} + F_D \cdot R_{BT} + F_A^{\text{Direct}} \quad [8]$$

where F_D^{noFRET} is the donor fluorescence without FRET, α is the ratio of the acceptor-to-donor quantum yields, R_{BT} is the fraction of bleed-through from the donor channel into the acceptor channel, F_A^{Direct} is the acceptor fluorescence due to direct excitation, and Y_{FRET} is the FRET efficiency. We can calculate the mean fluorescence lifetime, $\langle\tau\rangle$, using Eq. **6**, in which τ_D and τ_{AD} are the lifetimes of free donors and donors bound to acceptors, respectively. Here we assume that there are only 2 populations of donors.

Since Cerulean, the donor in the CFP-YFP version of EKAR, has a fluorescence decay curve with multiple time constants (1), it is difficult to estimate τ_D and τ_{AD} from fitting and therefore to estimate percent lifetime changes. We instead used values for a EGFP-mRFP1 pair. We used $\alpha = 0.4$ (22), $R_{BT} = 0.1$ (23), and $F_A^{\text{Direct}}/F_D^{\text{noFRET}} = 0.03$ (23), following previous measurements and simulations (21). For EGFP $\tau_D = 2.59$ ns (1), and from fitting (Eq. **4**) we estimated $\tau_{AD} = 1.1$. Since

$$Y_{\text{FRET}} = 1 - \frac{\tau_{AD}}{\tau_D} \quad [9]$$

we estimated $Y_{\text{FRET}} = 0.57$.

We set the initial binding fraction to 0.25 since

$$P_{AD} = \frac{\tau_D(\tau_D - \langle\tau\rangle)}{\tau_D(\tau_D - \langle\tau\rangle) + \tau_{AD}(\langle\tau\rangle - \tau_{AD})} \quad [10]$$

and $\langle\tau\rangle$ in the resting state for EKAR is ≈2.4 ns (Table S1). We calculated the percent lifetime and ratio changes following binding fraction increases between Δbinding fraction = 0 and Δbinding fraction = 0.2. For a fluorescence lifetime decrease of ≈3%, an acceptor-to-donor fluorescence ratio increase of ≈15% is expected (Fig. S2). For a CFP-YFP pair with $\alpha = 1.5$ (24), $R_{BT} = 0.2$ (24), and $F_A^{\text{Direct}}/F_D^{\text{noFRET}} = 0.03$ (23), a ratio increase of ≈20% is expected, assuming the same FRET efficiency. We therefore conclude that our experimentally measured relationship between lifetime and ratio changes is within an expected range for FRET changes.

1. Yasuda R, *et al.* (2006) Supersensitive Ras activation in dendrites and spines revealed by two-photon fluorescence lifetime imaging. *Nat Neurosci* 9:283–291.
2. Harvey CD, Svoboda K (2007) Locally dynamic synaptic learning rules in pyramidal neuron dendrites. *Nature* 450:1195–1200.
3. Mansour SJ, *et al.* (1994) Transformation of mammalian cells by constitutively active MAP kinase kinase. *Science* 265:966–970.
4. Gupta S, *et al.* (1996) Selective interaction of JNK protein kinase isoforms with transcription factors. *EMBO J* 15:2760–2770.
5. Bennett BL, *et al.* (2001) SP600125, an anthrapyrazolone inhibitor of Jun N-terminal kinase. *Proc Natl Acad Sci USA* 98:13681–13686.
6. Davies SP, Reddy H, Caivano M, Cohen P (2000) Specificity and mechanism of action of some commonly used protein kinase inhibitors. *Biochem J* 351:95–105.
7. Lakowicz JR (1999) *Principles of Fluorescence Spectroscopy* (Plenum, New York).
8. Becker W, *et al.* (2004) Fluorescence lifetime imaging by time-correlated single-photon counting. *Microsc Res Tech* 63:58–66.
9. Peter M, *et al.* (2005) Multiphoton-FLIM quantification of the EGFP-mRFP1 FRET pair for localization of membrane receptor-kinase interactions. *Biophys J* 88:1224–1237.
10. Baird GS, Zacharias DA, Tsien RY (1999) Circular permutation and receptor insertion within green fluorescent proteins. *Proc Natl Acad Sci USA* 96:11241–11246.
11. Nagai T, Sawano A, Park ES, Miyawaki A (2001) Circularly permuted green fluorescent proteins engineered to sense Ca2+. *Proc Natl Acad Sci USA* 98:3197–3202.
12. Nagai T, *et al.* (2004) Expanded dynamic range of fluorescent indicators for Ca2+ by circularly permuted yellow fluorescent proteins. *Proc Natl Acad Sci USA* 101:10554–10559.
13. Nguyen AW, Daugherty PS (2005) Evolutionary optimization of fluorescent proteins for intracellular FRET. *Nat Biotechnol* 23:355–360.
14. Ganesan S, *et al.* (2006) A dark yellow fluorescent protein (YFP)-based resonance energy-accepting chromoprotein (REACh) for Forster resonance energy transfer with GFP. *Proc Natl Acad Sci USA* 103:4089–14094.
15. Verdecia MA, *et al.* (2000) Structural basis for phosphoserine-proline recognition by group IV WW domains. *Nat Struct Biol* 7:639–643.
16. Zhang J, *et al.* (2005) Insulin disrupts beta-adrenergic signalling to protein kinase A in adipocytes. *Nature* 437:569–573.
17. Yasuda R, *et al.* (2004) Imaging calcium concentration dynamics in small neuronal compartments. *Sci STKE* 2004:pl5.
18. Arai R, *et al.* (2001) Design of the linkers which effectively separate domains of a bifunctional fusion protein. *Protein Eng* 14:529–532.
19. Fujioka A, *et al.* (2006) Dynamics of the Ras/ERK MAPK cascade as monitored by fluorescent probes. *J Biol Chem* 281:8917–8926.
20. Khokhlatchev AV, *et al.* (1998) Phosphorylation of the MAP kinase ERK2 promotes its homodimerization and nuclear translocation. *Cell* 93:605–615.
21. Yasuda R (2006) Imaging spatiotemporal dynamics of neuronal signaling using fluorescence resonance energy transfer and fluorescence lifetime imaging microscopy. *Curr Opin Neurobiol* 16:551–561.
22. Campbell RE, *et al.* (2002) A monomeric red fluorescent protein. *Proc Natl Acad Sci USA* 99:7877–7882.
23. Erickson MG, Moon DL, Yue DT (2003) DsRed as a potential FRET partner with CFP and GFP. *Biophys J* 85:599–611.
24. Tsien RY (1998) The green fluorescent protein. *Annu Rev Biochem* 67:509–544.
25. Sato M, *et al.* (2002) Fluorescent indicators for imaging protein phosphorylation in single living cells. *Nat Biotechnol* 20:287–294.
26. Mori MX, Erickson MG, Yue DT (2004) Functional stoichiometry and local enrichment of calmodulin interacting with Ca2+ channels. *Science* 304:432–435.

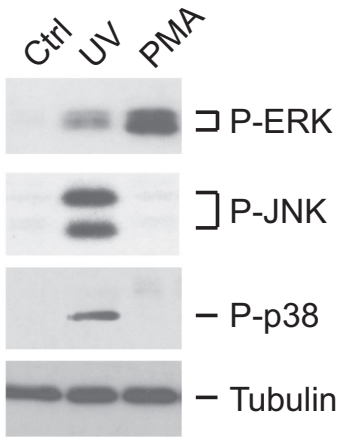

Fig. S1. Effect of UV and phorbol ester stimulation on MAPK activity in COS7 cells. COS7 cells were treated with 60 J/m^2 UV-C and then incubated for 1 h or treated with the phorbol ester PMA (1 μM) for 10 min. Protein extracts were examined by immunoblot analysis with antibodies to phospho-ERK, phospho-JNK, phospho-p38, and tubulin.

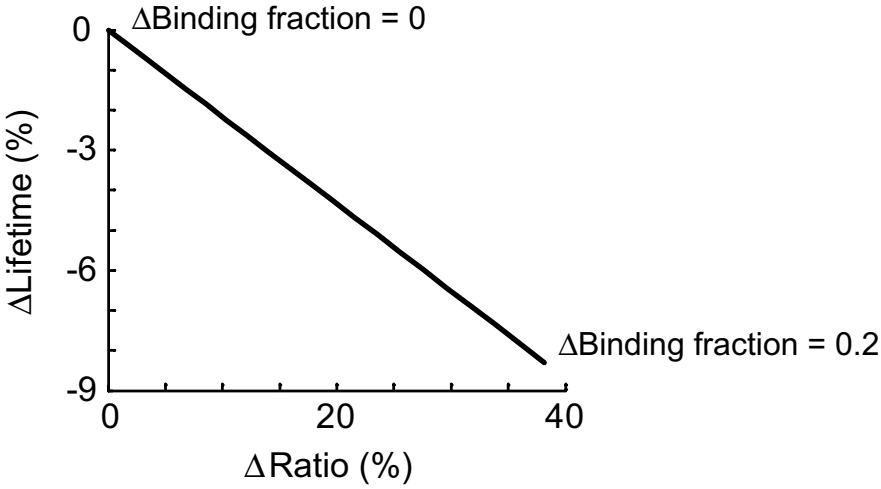

Fig. S2. Estimated percent changes in fluorescence lifetime and acceptor-to-donor fluorescence ratio for increases in binding fraction. Values are estimated for a EGFP-mRFP1 FRET pair. See *SI Text* for details.

Table S1. summary of tested sensors

	Baseline lifetime, ns	ΔLifetime[c], ns	ΔLifetime [c], %	Notes[d]
EKAR variants[a]				
EKAR cytoplasmic	2.41 ± 0.01	−0.071 ± 0.002	−2.92 ± 0.07	
EKAR nuclear	2.39 ± 0.01	−0.069 ± 0.003	−2.89 ± 0.15	
Intermolecular EKAR	2.56 ± 0.01	−0.009 ± 0.003	−0.35 ± 0.11	Cytoplasmic mRFP1-WW + Cdc25C-EGFP
FRET pairs[b]				
mRFP1-mRFP1-EGFP	2.28 ± 0.02	−0.073 ± 0.002	−3.20 ± 0.07	Two N-terminal copies of mRFP1
mRFP1-mVenus	2.79 ± 0.01	−0.051 ± 0.003	−1.82 ± 0.12	
mRFP1-cp49 Venus	2.93 ± 0.01	−0.094 ± 0.004	−3.21 ± 0.13	Nagai *et al.* (2004) *Proc Natl Acad Sci USA*
mRFP1-cp157 Venus	2.85 ± 0.02	−0.090 ± 0.008	−3.14 ± 0.31	Nagai *et al.* (2004) *Proc Natl Acad Sci USA*
mRFP1-cp173 Venus	2.77 ± 0.02	−0.070 ± 0.011	−2.53 ± 0.37	Nagai *et al.* (2004) *Proc Natl Acad Sci USA*
mRFP1-cp195 Venus	2.86 ± 0.01	−0.059 ± 0.007	−2.06 ± 0.27	Nagai *et al.* (2004) *Proc Natl Acad Sci USA*
mRFP1-cp229 Venus	2.88 ± 0.02	−0.070 ± 0.006	−2.44 ± 0.20	Nagai *et al.* (2004) *Proc Natl Acad Sci USA*
hcRed-Venus	2.83 ± 0.03	−0.017 ± 0.007	−0.58 ± 0.24	
mCherry-EGFP	2.43 ± 0.01	−0.068 ± 0.004	−2.80 ± 0.10	
EGFP-mRFP1	2.42 ± 0.01	−0.067 ± 0.001	−2.77 ± 0.06	Swap FP position in EKAR
mCerulean-mVenus	2.61 ± 0.03	−0.073 ± 0.009	−2.80 ± 0.34	
Phospho-binding and substrate peptides				
FHA phospho binding	2.47 ± 0.01	−0.032 ± 0.003	−1.31 ± 0.12	
RSK2 substrate	2.57 ± 0.01	−0.004 ± 0.002	−0.16 ± 0.10	Mouse RSK2 aa 560–740
Linkers				
Long linkers adjacent to FPs	2.43 ± 0.02	−0.015 ± 0.004	−0.63 ± 0.15	≈15-aa random sequence
9-aa central linker	2.36 ± 0.01	−0.041 ± 0.005	−1.72 ± 0.18	Sato *et al.* (2002) *Nat Biotechnol*
192 Gly linker	2.35 ± 0.01	−0.039 ± 0.004	−1.66 ± 0.17	Mori *et al.* (2004) *Science*
384 Gly linker	2.30 ± 0.02	−0.026 ± 0.007	−1.13 ± 0.20	Mori *et al.* (2004) *Science*
Helix central linker	2.35 ± 0.01	−0.052 ± 0.004	−2.21 ± 0.14	Arai *et al.* (2001) *Protein Eng*
Helix–Gly–Helix central linker	2.30 ± 0.03	−0.035 ± 0.006	−1.54 ± 0.19	
Gly–Helix–Gly central linker	2.33 ± 0.01	−0.038 ± 0.005	−1.63 ± 0.23	
Docking domains				
Cdc25C-FAFP	2.40 ± 0.02	−0.062 ± 0.004	−2.59 ± 0.17	
Cdc25C-FQAP	2.41 ± 0.02	−0.024 ± 0.005	−0.99 ± 0.22	
Cdc25C-ATAP	2.38 ± 0.02	−0.010 ± 0.003	−0.42 ± 0.11	
FQFP-Cdc25C-FQFP	2.36 ± 0.01	−0.068 ± 0.007	−2.89 ± 0.13	
Cdc25C-FQFP-FQFP	2.33 ± 0.01	−0.051 ± 0.010	−2.16 ± 0.31	
Cdc25C-linker-FQFP	2.44 ± 0.01	−0.026 ± 0.008	−1.08 ± 0.25	
Other sensor designs				
ERK dimerization	2.39 ± 0.01	−0.005 ± 0.002	−0.21 ± 0.09	mRFP-ERK-linker-EGFP-ERK
mRFP1-ERK-EGFP	2.41 ± 0.01	+0.013 ± 0.005	+0.56 ± 0.17	Based on Miu2; Fujioka *et al.* (2006) *J Biol Chem*

All data are mean ± SEM.

[a]All variants are version of nuclear EKAR with 1 component changed.

[b]The N-terminal fluorescent protein (FP) is listed first and the C-terminal FP is listed second (e.g. for EKAR: mRFP1-EGFP).

[c]Lifetime changes were measured in HEK293 cells following application of 100 ng/ml EGF.

[d]See references in *SI Text* for full citations.